## POLITECNICO DI TORINO
## Repository ISTITUZIONALE

Quench propagation in a TF coil of the EU DEMO

(Article begins on next page)

02 May 2024

# Accepted Manuscript

Title: Automated segmentation of brain cells for clonal analyses in fluorescence microscopy images

Authors: Massimo Salvi, Valentina Cerrato, Annalisa Buffo, Filippo Molinari

Please cite this article as: Salvi M, Cerrato V, Buffo A, Molinari F, Automated segmentation of brain cells for clonal analyses in fluorescence microscopy images, *Journal of Neuroscience Methods* (2019), https://doi.org/10.1016/j.jneumeth.2019.108348

**Article Type:** Research paper

# Automated segmentation of brain cells for clonal analyses in fluorescence microscopy images

Massimo Salvi[1], Valentina Cerrato[2], Annalisa Buffo[2], and Filippo Molinari[1]

[1] *Biolab, Department of Electronics and Telecommunications, Politecnico di Torino, Turin, Italy*

[2] *Department of Neuroscience Rita Levi-Montalcini, University of Turin and Neuroscience Institute Cavalieri Ottolenghi, Orbassano, Turin, Italy*

*CORRESPONDING AUTHOR**
Ing. M. Salvi
Biolab, Department of Electronics and Telecommunications, Politecnico di Torino, Torino, Italy.
Corso Duca degli Abruzzi, 24 - 10129 Torino, ITALY
Phone: 0039 011 090 4207
Fax: 0039 011 090 4217
E-mail: massimo.salvi@polito.it

**AUTHORS EMAIL**
Valentina Cerrato: valentina.cerrato@unito.it
Annalisa Buffo: annalisa.buffo@unito.it
Filippo Molinari: filippo.molinari@polito.it

## Highlights

- A fully automated method is presented for the segmentation of brain cells for clonal analysis in multi-channel fluorescence microscopy images.

- Clonal analysis represents a crucial tool in developmental biology to understand the ontogenesis of cell heterogeneity

- The proposed approach paves the way for future implementations aimed at realizing reliable systems integrating cell spatial contents for 3D reconstructions and multidimensional analyses.

## Abstract

The understanding of how cell diversity within and across distinct brain regions is ontogenetically achieved is a pivotal topic in neuroscience. Clonal analyses based on multicolor cell labeling represent a powerful tool to tackle this issue and disclose lineage relationships, but produce enormous sets of fluorescence images, leading to time consuming analyses that may be biased by the operator's subjectivity. Thus, time-efficient automated software are needed to analyze images easily, accurately and without subjective bias.

In this paper, we present a fully automated method, named FAST ('Fluorescent cell Analysis Segmentation Tool'), for the segmentation of neural cells labeled by multicolor combinations of fluorophores and for their classification into clones. The proposed method was tested on 77 high-magnification fluorescence images of adult mouse cerebellar tissues acquired using a confocal microscope. Automatic results were compared with manual annotations and two open-source software designed for cell detection in microscopic imaging. The algorithm showed very good performance in the cellular detection and in the assignment of the clonal identity.

To the best of our knowledge, FAST is the first fully automated technique for the analysis of cellular clones based on combinatorial expression of fluorescent proteins. The proposed approach allows to perform clonal analyses easily, accurately and objectively, overcoming those biases and errors that may result from manual annotations. Moreover, it can be broadly applied to the quantification and colocalization within cells of

fluorescent markers, therefore representing a versatile and powerful tool for automated quantitative analyses in fluorescence microscopy.

3

## Introduction

The technological advancements in multicolor labelling of cells and tissues, in association with modern semi-automated or automated microscopy, produce enormous sets of data. Looking at the resulting images by eye is extremely time consuming and subjectivity may introduce biases and errors in the analysis. Thus, many biologists find they need software to analyze images easily, accurately and objectively.

Clonal analyses, that allow to track the cell lineages derived from individual progenitors, currently represent a crucial tool in developmental biology to understand the ontogenesis of cell heterogeneity (Engstrom et al., 2002), (Espinet et al., 2000). To tackle this issue, in the neuroscience field, a specific method of lineage tracing employs genetic multicolored cell labeling. Indeed, with the development of distinct genetic tools allowing to permanently label the cells of interest, the idea of tracking entire lineages from their progenitors at high resolution first came true. The availability of a large variety of fluorescent reporters, together with the use of transgenic mice, triggered the idea of the use of conditional and combinatorial expression of different fluorescent proteins to define clonality of specific cell types. First, three distinct fluorescent reporters were combined to trace neurons (Feng et al., 2000), then, the Brainbow technology was designed to visualize synaptic circuits by genetically labeling individual neurons with as many as 90 distinguishable colors (Livet et al., 2007). Another clonal method employed stochastic recombination in isolated cells in distinct transgenic lines, as for mosaic analysis with double markers (MADM); (Zong et al., 2005), (Gao et al., 2014). Moreover, the three-lentiviral gene ontology (LeGO) vectors (Weber et al., 2011), (Weber et al., 2008) coding for red, green or blue (RGB) fluorescent proteins were developed and exploited to analyze clonal cell fates both in vitro and in vivo. To avoid the use of genetically modified organisms, DNA constructs encoding distinct fluorescent reporters were then designed to trace the lineage of single progenitors, following electroporation in the cells of interest (García-Marqués and López-Mascaraque, 2012), (García-Moreno et al., 2014), (Loulier et al., 2014), (Figueres-Oñate et al., 2016). Overall, multicolor reporter labelling is a powerful tool enabling the study of cell heterogeneity in a variety of settings, including developmental studies, analysis of stem cell functioning and tumorigenesis. Moreover, it finds

4

also applications in drug screening, where expression of distinct colors is designed to reveal specific cellular responses.

In all these examples, while large scale image acquisition is granted by the advancements of automated imaging, the identification of labelled cells and, thereafter, the recognition of different colors to define combinatorial codes or reveal changes of the cell status still largely rely on visual inspection and manual annotations.

In the last years, several methods have been proposed to perform cell segmentation in fluorescence microscopy images (Carpenter et al., 2006), (Coelho et al., 2009), (Alegro et al., 2017), (Ronneberger et al., 2015). However, many of these algorithms are semi-automatic (Schindelin et al., 2012), (Abràmoff et al., 2004), (Jurrus et al., 2013) and require user intervention to perform both an accurate segmentation of cells and their subsequent analysis (Amat et al., 2014), (Ortiz de Solorzano et al., 2001). On the other hand, fully automated algorithms are often bound to a specific application (Dima et al., 2011), (Dzyubachyk et al., 2008), (Longair et al., 2011), (Henry et al., 2013) and do not allow the integration of new modules (i.e. quantification of fluorescence expression). In addition, no fully automated solution was proposed so far for cell detection in multi-channel fluorescence microscopy images (Ulman et al., 2017), (Maška et al., 2014). Recent attempts to overcome these limitations include the generation of a macro integrated into ImageJ software (NIH) to facilitate the operator in the classification of the cells, based on the expression and intensity of expression of distinct fluorophores (Figueres-Oñate et al., 2016). However, in this case, selection of labelled cells still has to be done by the operator.

To the best of our knowledge, no full-automated solutions have been proposed so far for the analysis of cellular clones based on combinatorial expression of fluorescent proteins. In this paper, we show the FAST algorithm ('Fluorescent cell Analysis Segmentation Tool'), an adaptive and multi-channel method for the automatic segmentation of neural cells in fluorescence microscopy images and for their classification into clones. The proposed algorithm was tested on 77 images of mouse cerebral tissue and automatic results were compared with manual annotations of two expert biologists. In the following section, an exhaustive description of the method is presented.

5

## Materials and methods

### Image database

Our dataset consisted in 77 high-magnification images of adult (postnatal day 30, N=2) mouse cerebellar tissues, in which the UbC-*StarTrack* (Figueres-Oñate et al., 2016) or GFAP-*StarTrack* (Cerrato et al., 2018) methods were applied to perform clonal analysis and tracing of distinct cell types derived from single progenitors. In the second case, the images belonged to the same set of samples previously analyzed in (Cerrato et al., 2018). This technique takes advantage of the combinatorial expression in each cell of up to six fluorescent proteins to define clonality (Figueres-Oñate et al., 2016): mT-Sapphire (Ex. 399, Em. 511), mCerulean (Ex. 433, Em. 475), enhanced green fluorescent protein -EGFP- (Ex. 488, Em. 507), Yellow fluorescent protein -YFP- (Ex. 514, Em. 527), monomeric Kusabira Orange -mKO- (Ex. 548, Em. 559), mCherry (Ex. 587, Em. 610). Overall, the dataset contained images of several distinct cells' types of the mature cerebellum (either neurons or glial cells), that were distinguished and classified based on their diverse morphologies, localization within the tissue (Figure 1) and expression of cell/stage-specific markers.

Cerebella were isolated from mice after transcardial perfusion with 4% paraformaldehyde in 0.12 M phosphate buffer, pH 7.2–7.4, and stored overnight (o/n) in the same fixative at 4 °C. Cerebellar tissues were then embedded and frozen over dry ice in OCT (TissueTEK), sectioned in the parasagittal plane at 50 μm using a cryostat and put directly on glass slides. Slides were eventually mounted with Tris-glycerol supplemented with 10% Mowiol (Calbiochedm) and directly imaged. All images were acquired using a Leica TCS-SP5 confocal microscope, under fixed excitation and absorption conditions for each fluorophore, as previously described (García-Marqués and López-Mascaraque, 2012).
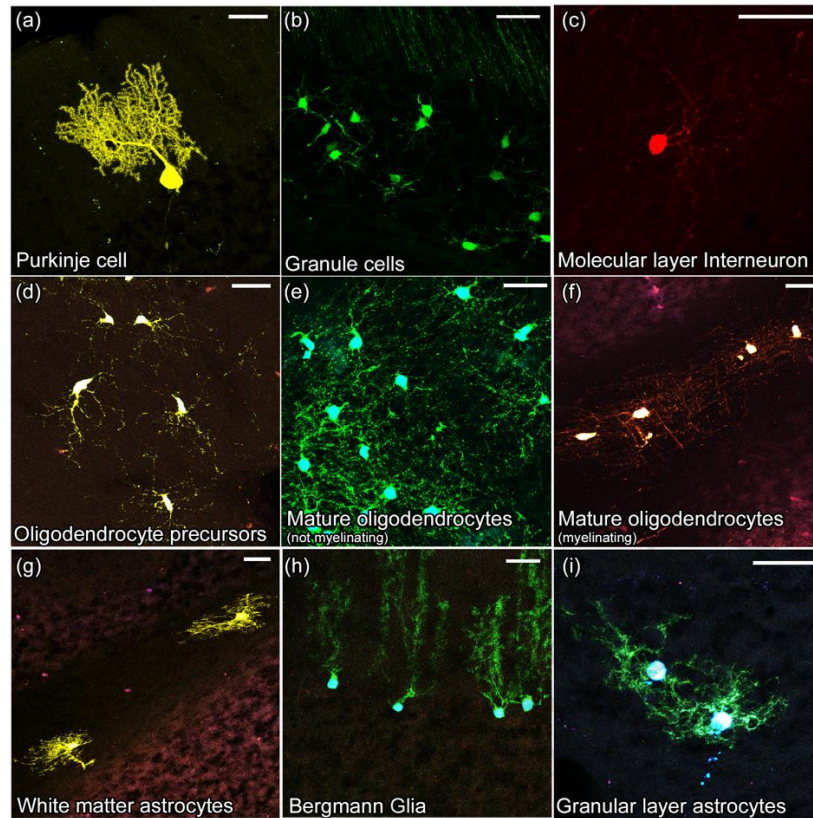
**Figure 1.** Representative images of the distinct cell types analyzed. The dataset contained images of diverse cerebellar cell types, clearly distinguishable according to their morphology and localization within the tissue. These cells comprised either neurons, such as Purkinje cells (a) and Granule cells (b), or interneurons (c), or glial cells (d-i). Glial cells included oligodendrocytes at distinct stages of maturation, i.e. precursors (d), mature not-myelinating (e) and mature myelinating oligodendrocytes (f), and the three main cerebellar astrocyte types, comprising white matter astrocytes (g), granular layer astrocytes (h) and Bergmann glia (i). Scale bars: 30μm.

The images were extracted from 31 mouse cerebellar slices and resulted from individual scans collected and digitalized at 40x magnification at the Neuroscience Institute Cavalieri Ottolenghi (Orbassano, Torino, Italy). Each image corresponded to a z-stack resulting from multiple steps 1.5 μm thick, whose total number varied according to the portion of tissue occupied by the labeled cells in each section. Images had a dimension of 1024x1024 pixels (resolution: 0.3784 μm/pixel). Our database contained 380 cells. A graphical user interface of the proposed method is available at https://data.mendeley.com/datasets/ yg6nfwm6cj/draft?a=688e8753-cfdd-43a5-8da8-8c2457b47efe.

7

## FAST algorithm architecture

The FAST algorithm is designed to automatically detect cells in fluorescence microscopy images. The algorithm was developed using MATLAB (MathWorks, Natick, MA, USA) environment and runs on a workstation with a 3.5 GHz octa-core CPU and 64-GB of RAM. The procedure of the proposed method is schematically described in Figure 2.
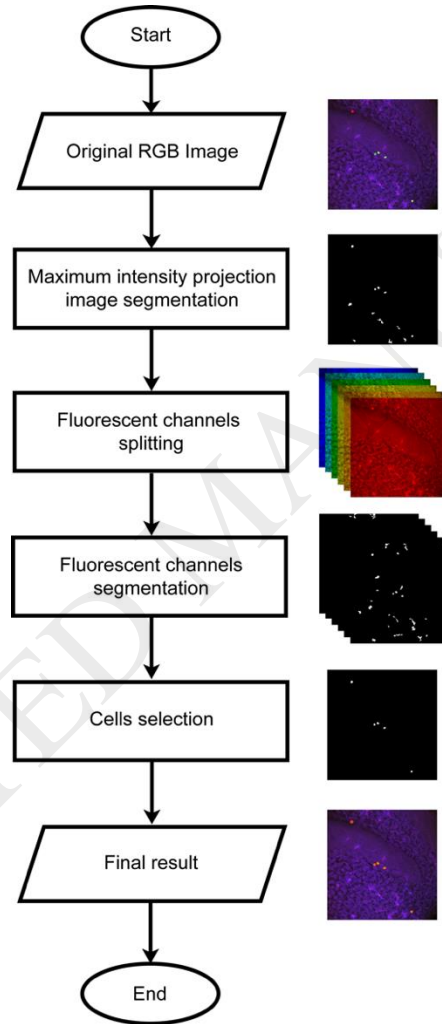


**Figure 2.** Schematic representation of the FAST algorithm.

Three main steps compose the processing: i) maximum intensity projection image segmentation, ii) fluorescent channels segmentation, iii) cells selection. In this section, a detailed description of the algorithm is provided.

8

**Maximum Intensity Projection image segmentation**

The proposed method takes as input the six image channels acquired using the confocal microscope: mT-Sapphire (blue), mCerulean (cyan), EGFP (green), YFP (yellow), mKO (orange), mCherry (red). Firstly, all six fluorescent channels are combined together to obtain the Maximum Intensity Projection (MIP) image.

The MIP image segmentation is performed using an object-based detection scheme adopted in our previous work (Salvi and Molinari, 2018), (Salvi et al., 2019). First of all, the pixel intensity values of the MIP image are normalized between 0 and 255. Then, the Progressive Weighted Mean ($PWM_{CURVE}$) of the grayscale histogram is computed. Considering a generic class P of the histogram ($0 \leq P \leq 255$), the value of $PWM_{CURVE}$ for that class is defined as:

$$PWM_{CURVE} = \frac{\sum_{i=0}^{P} w_i x_i}{\sum_{i=0}^{P} w_i}$$

where, $w_i$ is the histogram count for the $i^{th}$ class and $x_i$ is the respective bin gray intensity level. The $PWM_{CURVE}$ is evaluated for each class of the histogram as the weighted mean of all the grayscale histogram values up to that class. As the trend of $PWM_{CURVE}$ depends on the shape of the histogram, relevant features based on image color distribution can be extracted using this function. In particular, inflection points of $PWM_{CURVE}$ may be potential threshold values for performing cell segmentation, as they represent local stability points of the grayscale histogram. In particular, brain cellular clones can be defined as objects with an intensity higher than a threshold value that can be unambiguously identified as follows. First of all, the $PWM_{CURVE}$ is fitted with a $5^{th}$ order polynomial function with the aim to estimate its inflection points (*candidate thresholds*). Then, the MIP image is segmented using all the candidate thresholds and the median area of objects found is evaluated for all thresholds. Among candidate thresholds, the algorithm considers as *initial threshold* the one that identifies objects with the highest median area.

The processing steps for obtaining the initial threshold are illustrated in Figure 3, where three images with a high variation of laser intensities are used as example. The robustness of the proposed method can be

9

appreciated from Figure 3, where an optimal threshold was chosen, regardless the cell's appearance or histogram shapes.
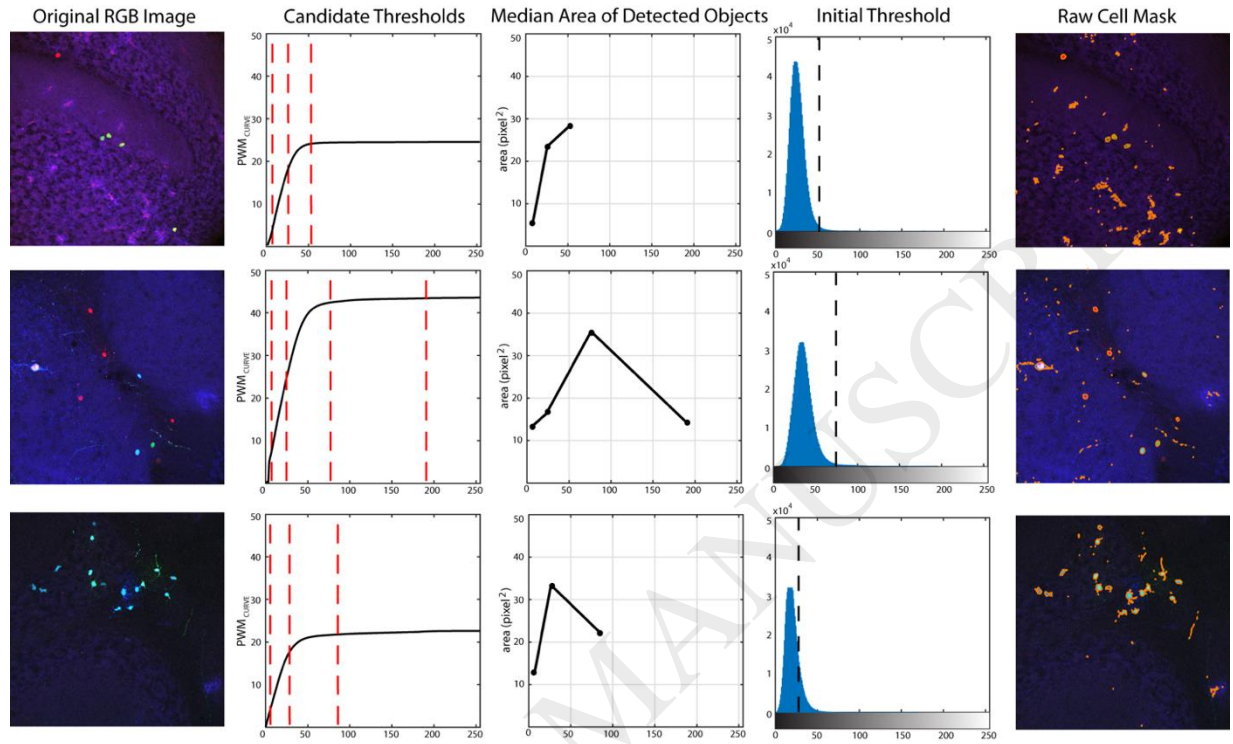


**Figure 3.** Processing for obtaining the initial threshold for different images of the stack with different high variation of intensity. The six fluorescent channels are combined to obtain the MIP (maximum intensity projection) image. Starting from the MIP image, the $PWM_{CURVE}$ is estimated from its grayscale histogram. Then, candidate thresholds are evaluated as inflection points of the curve (red dotted lines). The median area of detected objects using candidate threshold is calculated and the initial threshold is determined as the one with the highest median area. In the last column, the application of the initial threshold on the RGB image is shown.

The proposed method also includes an automatic strategy for the refinement of the shapes of the objects detected. Preliminarily, detected objects with area less than 7.15 $\mu m^2$ are deleted because they are too small to be considered as neural cells. Since it is expected that cells are convex objects, all regions with solidity less than 0.60 are erased from the mask. Solidity of a region is defined as the ratio between its area and convex area. Finally, a morphological dilation is carried out on the remaining objects, followed by a hole filling and a morphological erosion. A disk with radius equal to 2 pixels (equal to 0.7568 $\mu m$) is used as

10

structuring element for both dilation and erosion. With this operation, all previously segmented objects that for sure do not belong to cells are deleted.

The processing steps of the MIP image segmentation are shown in Figure 4. The result of the MIP image segmentation (*MIP_{mask}*) will be used in the following sections as starting point for cell detection.
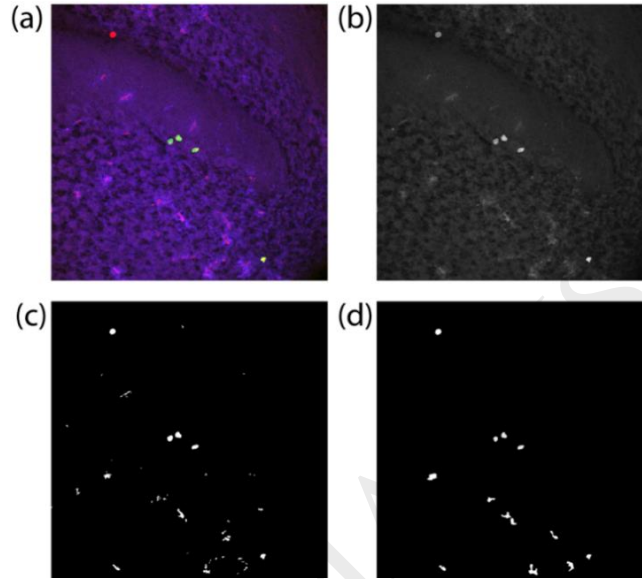


**Figure 4.** Maximum intensity projection image segmentation. (a) Original RGB image, (b) MIP image, (c) raw segmentation mask using the initial threshold, (d) segmentation mask after morphological cleaning (MIP_{mask}).

## Fluorescent channels segmentation

The *MIP_{mask}* might not be enough for the detection of all cells as a cell could be in principle labeled by any of the six fluorophores. For this reason, each fluorescent channel was analyzed to find out the presence of fluorescence signals. For each of the six fluorescent channels, the following five steps are performed:

1. image filtering using a median filter with a 5x5 kernel: this pre-processing step is carried out to reduce noise inside the channel image while preserving edges (Bankman, 2008);

2. application of the object-based detection described in the previous section to obtain a raw mask of neuronal cells within the fluorescent channel (Salvi and Molinari, 2018);

3. deletion of detected objects with area less than 7.15 $\mu m^2$ because they are too little to be considered candidate neural cells;

11

4. deletion of objects with eccentricity higher than 0.70. The eccentricity is the ratio of the distance between the foci of the ellipse that approximates the region and its major axis length. An object whose eccentricity is 0 is actually a circle, while an ellipse whose eccentricity is 1 is a line segment.

5. refining of objects shapes using morphological closing with a 3-pixels radius disk (equal to 1.15 µm). A morphological closing is a dilation followed by an erosion and it is used to obtain smoother region contours.

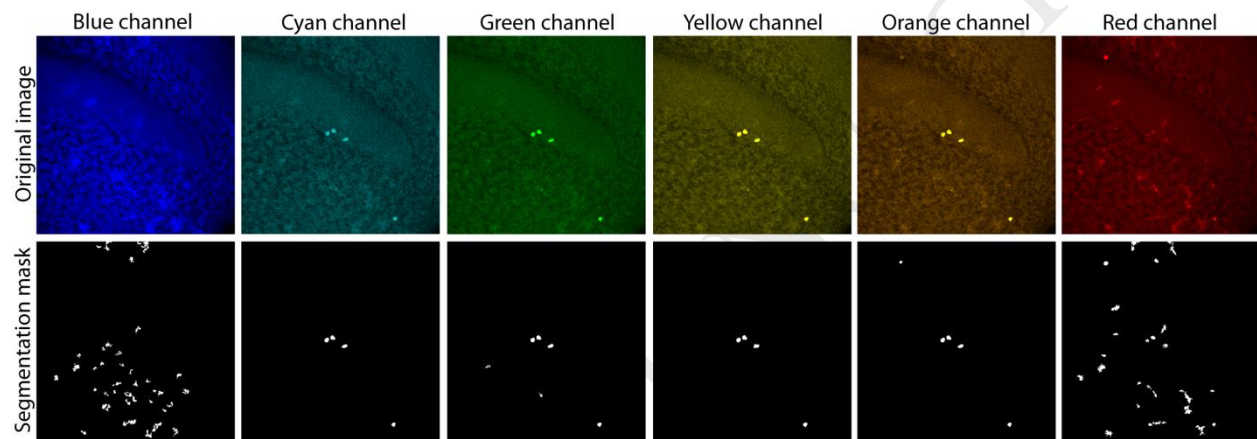The result of fluorescent channels segmentation is provided in Figure 5.



**Figure 5.** Fluorescent channels segmentation for the six fluorophores (columns). Original images and segmentation masks are shown in rows.

## Cells selection

In order to identify the cells, the six segmentation masks obtained in the previous section are combined together using the logical OR operator. The resulting mask contained all the objects present in at least one fluorescent channel (Figure 6a). Then, all regions with a solidity less than 0.60 are deleted because of their irregular shapes. The cleaned mask ($layer_{mask}$) contains all the objects that could be neural cells (Figure 6b). At this point of the processing, several conditions are imposed to $layer_{mask}$ to identify the real cells. A heuristic process based on six conditions is performed on each object of $layer_{mask}$. If at least five conditions are satisfied, the region is labeled as 'nervous cell', otherwise the object is deleted. The following six conditions are applied on each region of $layer_{mask}$:

12

1. object presence in $MIP_{mask}$: check if there is a region in the $MIP_{mask}$ that shares at least 75% of the object area;

2. contrast between object and its neighborhood: check if the region has an average grayscale intensity greater than 50% with respect to its contour;

3. object variance: check if the region has a grayscale intensity variance less than 0.05;

4. object presence in at least two fluorescent channels: check if there are two regions in the fluorescent segmentation masks that share at least 50% of the object area;

5. object size in fluorescent channels: check if the region has an area greater than 7.15 $\mu m^2$ in at least one of the fluorescent channels;

6. object intensity in fluorescent channels: check if the region has an average intensity greater than 200 (out of 255) in at least one of the fluorescent channels.

The result of cells selection is shown in Figure 6c, while the cell segmentation on the original RGB image is illustrated in Figure 6d.
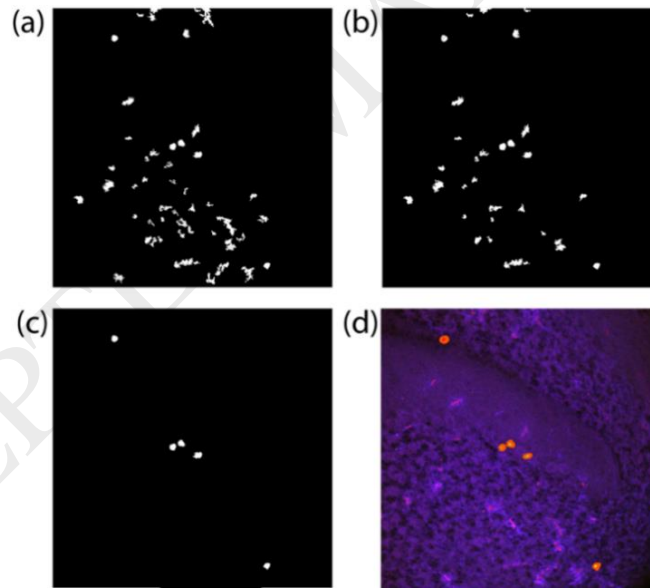


**Figure 6.** Cell selection. (a) mask obtained from the combination of the six fluorescent segmentation masks, (b) cleaned mask (layer$_{mask}$) after the removal of irregular shapes, (c) layer$_{mask}$ after cells selection, (d) final result on RGB image.

Once obtained the cellular mask, the FAST algorithm assigns a unique color-code to each cell. The lineage tracing strategy applied in the analyzed samples allows to define cells as part of a clone according to their combinatorial expression of the six abovementioned fluorescent proteins (i.e. cells with the same color

13

combination are part of the same clone) (Figueres-Oñate et al., 2016). To define the color combination of the identified cells, the presence of each cell in the six fluorescent channels is checked. If the following two conditions are satisfied, a neural cell will be considered present within a fluorescent channel:

1. contrast between object and its neighborhood: check if the region has an average fluorescent intensity greater than 25% with respect to its contour;

2. object variance: check if the region has a fluorescent intensity variance less than 0.10.

For each cell, the proposed method converts the combination of the six fluorescent reporter proteins into a six-number binary code, defined as:

$$color_{binary\ code} = b_6\ b_5\ b_4\ b_3\ b_2\ b_1$$

The order of fluorescent channels in the $color_{binary\ code}$ is determined by the confocal acquisition parameters ($b_6$-blue; $b_5$-cyan; $b_4$-green; $b_3$-yellow; $b_2$-orange; $b_1$-red). 1 indicates the presence of the neuronal clone in the current fluorescent channel while 0 represents the absence of a fluorescent signal. For example, if a cellular clone express fluorescence in the green, yellow and red channels, its $color_{binary\ code}$ will be 001101.

## Performance measures

The parameters tuning of the CARE algorithm is reported in Appendix. Automatic results provided by FAST were compared with manual segmentations. Two manual operators with more than 8 years of experience in neuroscience (named OP1 and OP2), manually draw each cell to assess inter-operator variability in the cell detection. True positive (TP) represents the number of cells identified by FAST with an overlap higher than 80% with the manual cells. False negative (FN) denotes all cells not found by the automatic method (or with an overlap lower than 20% with the manual cells). False positive (FP) represents all cells obtained by FAST without a corresponding manual drawing.

The performance of cells detection was evaluated by calculating the *recall*, *precision* and *F1-score*, which are defined as follows:

$$recall = \frac{TP}{TP + FN}$$

14

$$precision = \frac{TP}{TP + FP}$$

$$F1_{SCORE} = \frac{2 \text{ x } (recall \text{ x } precision)}{(recall + precision)}$$

*Recall* assesses the missed detection of ground truth objects (manual cells) while *precision* evaluates the false detection of ghost objects. $F1_{SCORE}$ is defined as the harmonic mean of *recall* and *precision*. $F1_{SCORE}$ is a common used object detection metric (Malon and Cosatto, 2013), but it penalizes only object-level errors (Kumar et al., 2017). To evaluate the accuracy of the segmentation, *SDC* (Sorensen-Dice Coefficient) and *HD* (Hausdorff Distance) were also evaluated:

$$SDC = \frac{2 |A \cap B|}{|A| + |B|}$$

$$HD_{(a \in A, b \in B)} = \max\{d(a, b)\}$$

where *A* is the manual cell shape drawn by the operator, *B* is the cell identified by the algorithm and *d(a,b)* is the distance between point a (on border of shape *A*) and point b (on border of shape *B*). *SDC* measures similarity between two different shapes, defined as twice the size of their intersection divided by the sum of the two shapes areas (Zou et al., 2004). *HD* measures how far two borders are from each other. Two contours are close in the Hausdorff distance if every point of either set is close to some point of the other set (Huttenlocher et al., 1993).

Automatic $color_{binary\ code}$ provided by FAST was also compared with manual $color_{binary\ code}$ made by two expert operators (OP1 and OP2). The agreement between manual and automatic $color_{binary\ code}$ was evaluated by calculating the *CCA* (*color-code agreement*), which is defined as:

$$CCA = \frac{\sum_{bitwise}(bc_{manual} \odot bc_{automatic})}{\# \ fluorescent \ channels} \ x \ 100$$

where $\odot$ is the XNOR operator, $bc_{manual}$ is the $color_{binary\ code}$ provided by the manual operator and $bc_{automatic}$ is the automatic $color_{binary\ code}$. The *CCA* is defined between 0% and 100%. A *CCA* equal

15

to 0% indicates two complementary $color_{binary\ codes}$ while a value of 100% represents two identical $color_{binary\ codes}$.

## Results

### Comparison with manual operator

The performance of the proposed method in cell detection is summarized in Table 1 while the segmentation accuracy of FAST is reported in Table 2.

FAST demonstrated to offer excellent performances in cell detection, with high average values of *precision*, *recall* and *F1$_{SCORE}$* (Table 1). The average *F1$_{SCORE}$* calculated between the two operators (0.9275) is comparable with the one obtained between FAST and each of them (0.9032 and 0.9154). The proposed algorithm also showed very high values of *SDC* thus demonstrating the accuracy of the method (Table 2). In addition, the mean Hausdorff distance (*HD*) was always lower than 2 μm.

The average *CCA* calculated between the two operators (96.25%) was comparable with the one obtained between FAST and each of them (96.42% and 94.72%), thereby indicating the reliability of the algorithm in the assignment of clonal identity (defined by the $color_{binary\ code}$) to the detected cells. We also evaluated the percentage of color agreement between the two operators and our algorithm in each of the six fluorescent channels (e.g. both agreed that red color was present/absent within a detected cell). The results are summarized in Table 3.

A very strong agreement was observed for the blue channel (OP1vs FAST: 100%, OP2vs FAST: 99.09%) while the lowest value was obtained for the cyan channel (OP1vs FAST: 91.78%, OP2vs FAST:92.09%). Since the cyan layer has often a lower contrast compared to the other fluorescent channels (see the first row of Figure 5), the manual operators may have more difficulty in verifying the presence/absence of this color inside a detected cell.

16

Finally, a Kruskal-Wallis test (Breslow, 1970) is used to compare the inter-operator variability (OP1vsOP2) with the automatic performance (OP1vsFAST, OP2vsFAST). The Kruskal-Wallis test works under the null-hypothesis that the data comes from the same distribution (p-value was set to 0.05). The Kruskal-Wallis test confirmed that there was no statistical difference between inter-operator variability (OP1vsOP2) and automatic performance (OP1vs FAST, OP2vs FAST) for both SDC and CCA (p-value > 0.05).

An explanatory example comparing the output of the segmentation obtained by applying FAST and by manual operators is presented in Figure 7.
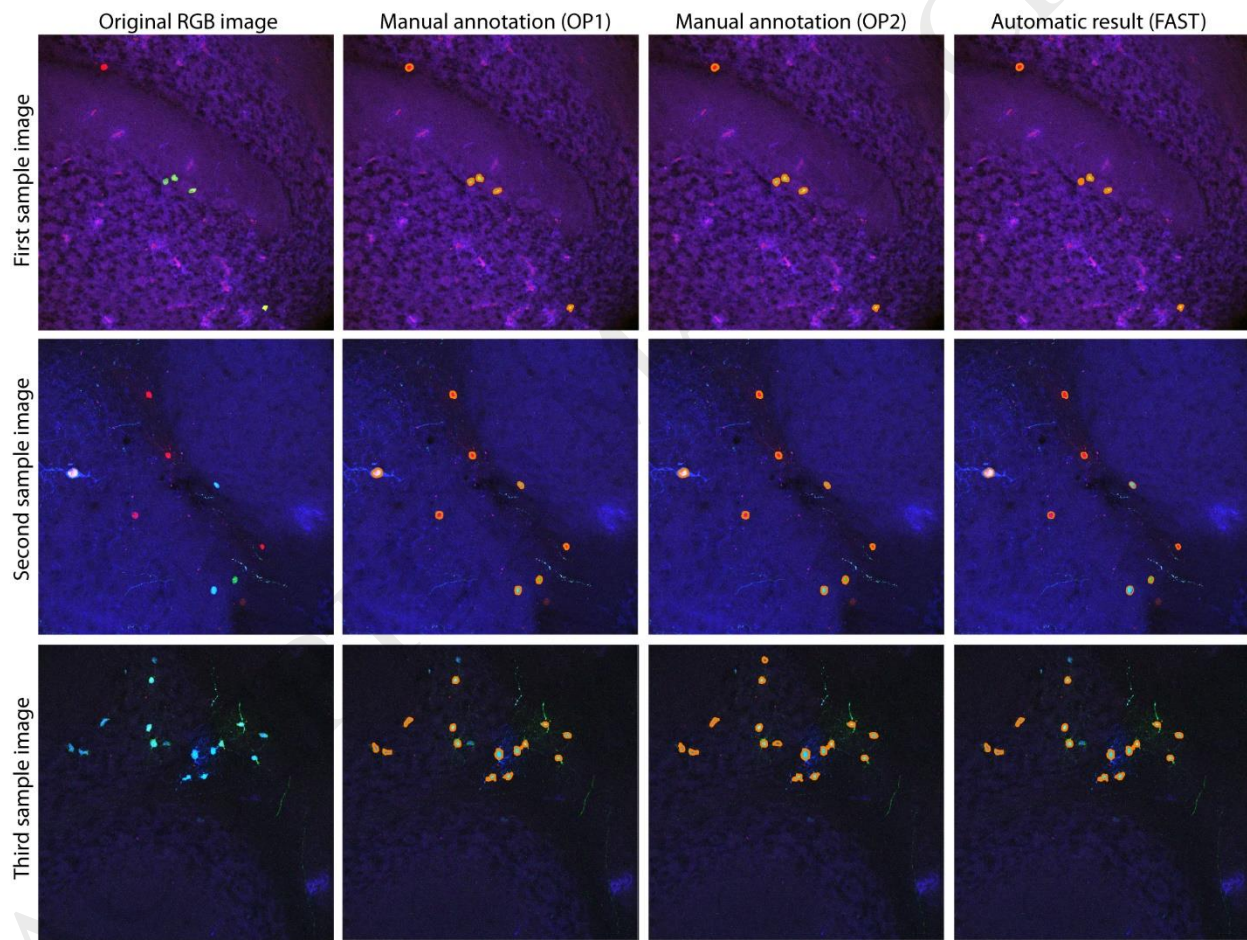


**Figure 7.** Comparison between manual and automatic segmentation for three samples (rows), showing images with a high variation of laser intensities and cells appearance. The original RGB image, manual annotations (OP1 and OP2) and automatic segmentation are shown in columns.

**Comparison with open-source software**

17

The results obtained by the proposed algorithm were also compared with two open-source software (CellProfiler and Fiji) widely applied to the analysis of fluorescence microscopy images. CellProfiler (Carpenter et al., 2006) is a software designed to measure and analyse cell images. This program is composed of a series of image-processing modules that allow the user to perform an automatic analysis (plugin used: UnmixColors, Threshold, ImageMath, IdentifyPrimaryObjects, ConvertObjectsToImage). The pipeline implemented in CellProfiler is the same one used for cell segmentation in a previous work (Buggenthin et al., 2013). The following modules were sequentially called for each image: UnmixColors (Custom Stain, Red/Green/Blue absorbance: 0.497, 0.728, 0.469, respectively); Threshold (Adaptive threshold strategy, Otsu method with two class); ImageMath (Invert Operation); IdentifyPrimaryObjects (Typical diameter of cells: 15 to 100, splitting method: Intensity, method to draw dividing lines: Shape), Convert objects to image (saved binary mask).

Fiji (Schindelin et al., 2012) is a Java-based software with several plugins which facilitate scientific image analysis (Healy et al., 2018). Our Fiji pipeline is based on a semi-automatic processing consisting of: (i) manual intensity color thresholding (Image>Adjust>Color Threshold; Color space: RGB), (ii) conversion into binary mask (Process>Binary>Make Binary), (iii) hole filling (Process>Binary>Fill Holes) and (iv) small particles removal (Analyze>Analyze Particles; Size: 7.15 $\mu m^2$-Infiity; Circularity: 0.25-1.00).

A visual inspection of Figure 8 allows to compare the performances of CellProfiler, Fiji and FAST in neuronal cell segmentation. A quantitative comparison of the performances offered by the two open-source software with FAST is reported in Table 4 and Table 5.
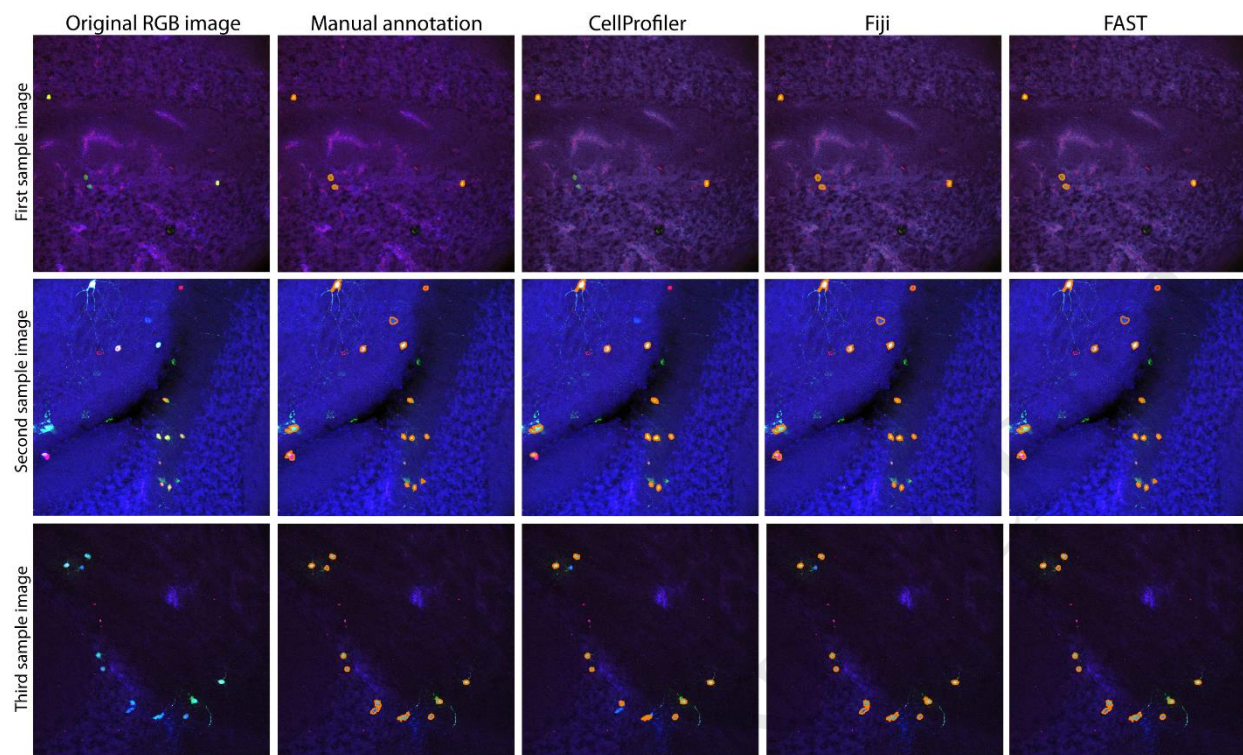
18

**Figure 8.** Comparison between two open-source software and the proposed method for three samples (rows). The segmentation masks provided by CellProfiler, Fiji and FAST are shown in columns.

As can be seen from Table 4, the Cell Profiler segmentation is characterized by a low *recall* for both operators (0.6157 and 0.5974) and this leads to a lowering of the average $F1_{SCORE}$ (0.7571 and 0.7418). The CellProfiler pipeline allowed to obtain the lowest number of FP cells (4 and 5) but many cells were missed (FN: 146 and 153). Moreover, the mean *SDC* was lower than the proposed one for more than 10% (Table 5).

Fiji segmentation performance is quite similar to FAST results. The average F1-score achieved with Fiji was comparable to that obtained with FAST (0.9236 and 0.9143 vs 0.9034 and 0.9154). Importantly, however, Fiji is a semi-automatic software and requires user intervention to function properly. For this reason, the average computational time is about 7 times higher than FAST algorithm.

## Discussion

In the present study, we proposed a fully automatic method for the segmentation of neural cells in multi-channel fluorescence microscopy images and for their classification into clones according to the

combinatorial expression of distinct fluorescent proteins.

Due to the huge heterogeneity within both progenitor and mature cell pools, the understanding of how cell diversity is ontogenetically achieved is a pivotal issue in neuroscience and, in general, in developmental biology. In this context, clonal analyses based on stochastic multicolor cell labeling are a very powerful tool now widely applied to decipher with high accuracy clonal relationships among and within type- or region-specific kinds of cells in defined systems, and to disclose the functional implications of cell heterogeneity in both physiology and pathology. This kind of analysis produces a large amount of data, mostly in the form of confocal images, in which the labeled cells have been so far manually identified and classified by the operator with only partial help by semi-automated tools, thereby introducing possible biases and leading to time consuming analyses.

To the best of our knowledge, FAST is the first fully automated solution for the analysis of cellular clones based on combinatorial expression of fluorescent proteins. The proposed method is able to recognize brain cells inside fluorescence images with no requirement of any user interaction. The algorithm was tested on 77 high-magnification images of mouse cerebellar tissues, in which the UbC-StarTrack (Figueres-Oñate et al., 2016) or GFAP-StarTrack (Cerrato et al., 2018) methods were applied to perform clonal analysis and tracing of several distinct cell types derived from single progenitors. For all the images of our dataset, two expert biologists manually annotated the cells and assigned a unique color-code to each of them. The comparison between manual and automatic segmentation confirmed high performances for the proposed approach.

The observed robustness of FAST algorithm with respect to the cell appearance variability was mainly due to the implementation of adaptive thresholding and of an optimized cell selection. In addition, the mean color-code agreement assessed between the two operators (96.25%) was also analogous with the one achieved between the proposed algorithm and each operator (96.42% and 96.35%). The FAST algorithm allowed also to obtain: (1) the highest average $F1_{SCORE}$ (best object detection) compared to other open-source software designed for cell detection in fluorescence microscopy; (2) the lowest running time and,

20

respect to other automatic and semi-automatic methods, the shortest Hausdorff distance (best segmentation accuracy).

Importantly, the algorithm can unequivocally distinguish among distinct levels of fluorescence, which could suffer heavy subjective biases during manual annotations. This is particularly important when exploiting clonal analysis tools, such as the UbC- and GFAP-StarTrack, in which the clonal identity is not only defined by the presence of specific fluorescent reporter proteins, but also by their expression levels (which, in methods based on the integration of expression constructs, is meant to correspond to the number of integrated copies (Figueres-Oñate et al., 2016)).

Of note, this algorithm combines for the first time the fully automated segmentation of cells to the detection, within each cell, of the expressed fluorescent proteins, thereby leading to a color code indicative of the clonal identity of the cell (i.e. cells with the same color code are sister cells). This results in a fully automated analysis, with no need for the operator's intervention until data are ready to be organized and interpreted. Through the proposed method, considerable amounts of data can thereafter be easily handled and automatically and rapidly processed according to the user's needs. For instance, important aspects in clonal analysis are the evaluation of the composition of clones, their frequency and their size in terms of both cell number and spatial dispersion. With respect to this last issue, FAST automatic segmentation can provide the spatial coordinates of the cells within serial sections of the tissue of interest and then perform 3D reconstructions of the clones, with further applications in spatial analyses (such as cluster and Nearest Neighbor Distance analyses, prediction of migratory routes from the site of origin). Importantly, although the algorithm was tested in a single mouse brain region, the cerebellum, the cells subjected to analysis covered a wide range of types (from neurons, to astrocytes and oligodendrocytes) and subtypes (i.e. three kinds of interneurons, granule and Purkinje neurons, three types of astrocytes, mature and immature oligodendrocytes) with their own specific morphologies and soma diameters spanning from approximately 10 to 20µm (Leto et al., 2016) as shown in Figure 1. The FAST method is therefore very likely to be applicable to the segmentation and analysis of either neural or non-neural cells in any region of interest. Moreover, thanks to the reliable cell detection provided by FAST, the proposed algorithm can also be

21

applied for the quantification and the colocalization of fluorescently labeled markers within cell somata in conventional immunocytochemistry and immunohistochemistry.

## Conclusion

In this paper, an adaptive method for neural cell segmentation in fluorescence microscopy images is presented. To the best of our knowledge, FAST is the first fully automated solution for the analysis of cellular clones based on combinatorial expression of fluorescent proteins.

The algorithm was tested on 77 high-magnification images of mouse cerebral tissue, in which cell nuclei had different intensities, shapes and dimensions. High segmentation performances were obtained and, for each image of the dataset, the algorithm took around 5 seconds to perform cellular clone segmentation, thus indicating the efficiency of the proposed technique.

Being totally automated, this algorithm first overcomes all those issues related to time consuming manual annotations and analyses in fluorescence microscopy images, thereby significantly enhancing the efficiency of multicolor-based cell analyses. Moreover, it represents the starting point for future implementations aimed at realizing reliable systems integrating cell spatial contents for 3D reconstructions and multidimensional analyses.

## Appendix

To optimize the performance of the proposed method, we conducted a sensitivity analysis on the main parameters that the FAST algorithm features: polynomial$_{ORDER}$ (order of the polynomial function that fit the PWM$_{CURVE}$), small$_{OBJECTS}$ (minimum area of detected objects), min$_{SOLIDITY}$ (minimum solidity of a segmented region to be considered as nervous cell) and num$_{CONDITIONS}$ (minimum number of conditions to be satisfied during the cell selection). The sensitivity analysis of the FAST algorithm is outlined in Table 6.

22

To evaluate the performance, we calculated the $F1_{SCORE}$ between the automatic and manual segmentations of two operators. As optimal parameters, we chose those that maximized the $F1_{SCORE}$ values between FAST and the two manual operators (operator 1 and 2).

The polynomial$_{ORDER}$ is the most crucial parameter used by the object-based detection adopted for MIP and fluorescent channels segmentation. Low values of this parameter (e.g. 3) may not provide a good 'fit' of the $PWM_{CURVE}$ function, while too high values of polynomial$_{ORDER}$ (e.g. 7) can generate 'ghost' inflection points due to mathematical interpolation. For this application, the polynomial$_{ORDER}$ that guarantees the best $F1_{SCORE}$ is 5.

The minimum area of detected objects (small$_{OBJECTS}$) influences the cleaning step during the cell detection in all six fluorescent channels. A low small$_{OBJECTS}$ value of 2.86 $\mu m^2$ does not allow to remove all the 'not-cell' objects, causing a high number of false positive regions that lower the $F1_{SCORE}$. On the other hand, increasing the value of small$_{OBJECTS}$ to 14.30 $\mu m^2$ would lead to the removal of actual neural cells, causing a rise of the true negative regions.

Finally, we tested three values of num$_{CONDITION}$ (4/6, 5/6, 6/6) during the cell selection step. The FAST algorithm is very sensitive if only 4 out of 6 conditions should be satisfied during the cell selection. Using this value, the method is less restrictive and a great number of false positive regions are not deleted, causing a large decrease of F1score. If all the six condition (6/6) had to be satisfied to label a region as 'nervous cell', the FAST algorithm is characterized by high precision (very low FP regions) but several neural cells are not detected (high number of FN objects). This result suggests and confirms that a value of num$_{CONDITION}$ equal to 5/6 is the best compromise, allowing the highest performance in the brain cells segmentation.

23

# References

Abràmoff, M.D., Magalhães, P.J., Ram, S.J., 2004. Image processing with ImageJ. Biophotonics Int. 11, 36–42.

Alegro, M., Theofilas, P., Nguy, A., Castruita, P.A., Seeley, W., Heinsen, H., Ushizima, D.M., Grinberg, L.T., 2017. Automating cell detection and classification in human brain fluorescent microscopy images using dictionary learning and sparse coding. J. Neurosci. Methods 282, 20–33.

Amat, F., Lemon, W., Mossing, D.P., McDole, K., Wan, Y., Branson, K., Myers, E.W., Keller, P.J., 2014. Fast, accurate reconstruction of cell lineages from large-scale fluorescence microscopy data. Nat. Methods 11, 951.

Bankman, I., 2008. Handbook of medical image processing and analysis. Elsevier.

Breslow, N., 1970. A generalized Kruskal-Wallis test for comparing K samples subject to unequal patterns of censorship. Biometrika 57, 579–594.

Buggenthin, F., Marr, C., Schwarzfischer, M., Hoppe, P.S., Hilsenbeck, O., Schroeder, T., Theis, F.J., 2013. An automatic method for robust and fast cell detection in bright field images from high-throughput microscopy. BMC Bioinformatics 14, 297.

Carpenter, A.E., Jones, T.R., Lamprecht, M.R., Clarke, C., Kang, I., Friman, O., Guertin, D.A., Chang, J., Lindquist, R.A., Moffat, J., Golland, P., Sabatini, D.M., 2006. CellProfiler: image analysis software for identifying and quantifying cell phenotypes. Genome Biol. 7, R100. https://doi.org/10.1186/gb-2006-7-10-r100

Cerrato, V., Parmigiani, E., Figueres-Oñate, M., Betizeau, M., Aprato, J., Nanavaty, I., Berchialla, P., Luzzati, F., de'Sperati, C., Lopez-Mascaraque, L., 2018. Multiple origins and modularity in the spatiotemporal emergence of cerebellar astrocyte heterogeneity. PLoS Biol. 16, e2005513.

Coelho, L.P., Shariff, A., Murphy, R.F., 2009. Nuclear segmentation in microscope cell images: a hand-segmented dataset and comparison of algorithms, in: Biomedical Imaging: From Nano to Macro, 2009. ISBI'09. IEEE International Symposium On. IEEE, pp. 518–521.

Dima, A.A., Elliott, J.T., Filliben, J.J., Halter, M., Peskin, A., Bernal, J., Kociolek, M., Brady, M.C., Tang, H.C., Plant, A.L., 2011. Comparison of segmentation algorithms for fluorescence microscopy images of cells. Cytom. Part A 79, 545–559.

Dzyubachyk, O., Niessen, W., Meijering, E., 2008. Advanced level-set based multiple-cell segmentation and tracking in time-lapse fluorescence microscopy images, in: Biomedical Imaging: From Nano to Macro, 2008. ISBI 2008. 5th IEEE International Symposium On. IEEE, pp. 185–188.

Engstrom, C.M., Demers, D., Dooner, M., McAuliffe, C., Benoit, B.O., Stencel, K., Joly, M., Hulspas, R., Reilly, J.L., Savarese, T., 2002. A method for clonal analysis of epidermal growth factor-responsive neural progenitors. J. Neurosci. Methods 117, 111–121.

Espinet, C., Gómez-Arbonés, X., Egea, J., Comella, J.X., 2000. Combined use of the green and yellow fluorescent proteins and fluorescence-activated cell sorting to select populations of transiently transfected PC12 cells. J. Neurosci. Methods 100, 63–69.

Feng, G., Mellor, R.H., Bernstein, M., Keller-Peck, C., Nguyen, Q.T., Wallace, M., Nerbonne, J.M., Lichtman, J.W., Sanes, J.R., 2000. Imaging neuronal subsets in transgenic mice expressing multiple spectral variants of GFP. Neuron 28, 41–51.

Figueres-Oñate, M., García-Marqués, J., López-Mascaraque, L., 2016. UbC-StarTrack, a clonal method to target the entire progeny of individual progenitors. Sci. Rep. 6, 33896.

Gao, P., Postiglione, M.P., Krieger, T.G., Hernandez, L., Wang, C., Han, Z., Streicher, C., Papusheva, E., Insolera, R., Chugh, K., 2014. Deterministic progenitor behavior and unitary production of neurons in the neocortex. Cell 159, 775–788.

García-Marqués, J., López-Mascaraque, L., 2012. Clonal identity determines astrocyte cortical heterogeneity. Cereb. cortex 23, 1463–1472.

García-Moreno, F., Vasistha, N.A., Begbie, J., Molnár, Z., 2014. CLoNe is a new method to target single progenitors and study their progeny in mouse and chick. Development 141, 1589–1598.

Healy, S., McMahon, J., Owens, P., Dockery, P., FitzGerald, U., 2018. Threshold-based segmentation of fluorescent and chromogenic images of microglia, astrocytes and oligodendrocytes in FIJI. J. Neurosci. Methods 295, 87–103.

Henry, K.M., Pase, L., Ramos-Lopez, C.F., Lieschke, G.J., Renshaw, S.A., Reyes-Aldasoro, C.C., 2013. PhagoSight: an open-source MATLAB® package for the analysis of fluorescent neutrophil and macrophage migration in a zebrafish model. PLoS One 8, e72636.

Huttenlocher, D.P., Klanderman, G.A., Rucklidge, W.J., 1993. Comparing images using the Hausdorff distance. IEEE Trans. Pattern Anal. Mach. Intell. 15, 850–863.

Jurrus, E., Watanabe, S., Giuly, R.J., Paiva, A.R.C., Ellisman, M.H., Jorgensen, E.M., Tasdizen, T., 2013. Semi-automated neuron boundary detection and nonbranching process segmentation in electron microscopy images. Neuroinformatics 11, 5–29.

Kumar, N., Verma, R., Sharma, S., Bhargava, S., Vahadane, A., Sethi, A., 2017. A Dataset and a Technique for Generalized Nuclear Segmentation for Computational Pathology. IEEE Trans. Med. Imaging 36, 1550–1560. https://doi.org/10.1109/TMI.2017.2677499

Leto, K., Arancillo, M., Becker, E.B.E., Buffo, A., Chiang, C., Ding, B., Dobyns, W.B., Dusart, I., Haldipur, P., Hatten, M.E., 2016. Consensus paper: cerebellar development. The Cerebellum 15, 789–828.

Livet, J., Weissman, T.A., Kang, H., Draft, R.W., Lu, J., Bennis, R.A., Sanes, J.R., Lichtman, J.W., 2007. Transgenic strategies for combinatorial expression of fluorescent proteins in the nervous system. Nature 450, 56.

Longair, M.H., Baker, D.A., Armstrong, J.D., 2011. Simple Neurite Tracer: open source software for reconstruction, visualization and analysis of neuronal processes. Bioinformatics 27, 2453–2454.

Loulier, K., Barry, R., Mahou, P., Le Franc, Y., Supatto, W., Matho, K.S., Ieng, S., Fouquet, S., Dupin, E., Benosman, R., 2014. Multiplex cell and lineage tracking with combinatorial labels. Neuron 81, 505–520.

Malon, C.D., Cosatto, E., 2013. Classification of mitotic figures with convolutional neural networks and seeded blob features. J. Pathol. Inform. 4, 9. https://doi.org/10.4103/2153-3539.112694

Maška, M., Ulman, V., Svoboda, D., Matula, Pavel, Matula, Petr, Ederra, C., Urbiola, A., España, T., Venkatesan, S., Balak, D.M.W., 2014. A benchmark for comparison of cell tracking algorithms. Bioinformatics 30, 1609–1617.

Ortiz de Solorzano, C., Malladi, R., Lelievre, S.A., Lockett, S.J., 2001. Segmentation of nuclei and cells using membrane related protein markers. J. Microsc. 201, 404–415.

Ronneberger, O., Fischer, P., Brox, T., 2015. U-net: Convolutional networks for biomedical image segmentation, in: International Conference on Medical Image Computing and Computer-Assisted Intervention. Springer, pp. 234–241.

Salvi, M., Molinari, F., 2018. Multi-tissue and multi-scale approach for nuclei segmentation in H&E stained images. Biomed. Eng. Online 17, 89. https://doi.org/10.1186/s12938-018-0518-0

Salvi, M., Morbiducci, U., Amadeo, F., Santoro, R., Angelini, F., Chimenti, I., Massai, D., Messina, E., Giacomello, A., Pesce, M., 2019. Automated Segmentation of Fluorescence Microscopy Images for 3D Cell Detection in human-derived Cardiospheres. Sci. Rep. 9, 6644.

Schindelin, J., Arganda-Carreras, I., Frise, E., Kaynig, V., Longair, M., Pietzsch, T., Preibisch, S., Rueden, C., Saalfeld, S., Schmid, B., Tinevez, J.-Y., White, D.J., Hartenstein, V., Eliceiri, K., Tomancak, P., Cardona, A., 2012. Fiji: an open-source platform for biological-image analysis. Nat. Methods 9, 676–682. https://doi.org/10.1038/nmeth.2019

Ulman, V., Maška, M., Magnusson, K.E.G., Ronneberger, O., Haubold, C., Harder, N., Matula, Pavel, Matula, Petr, Svoboda, D., Radojevic, M., 2017. An objective comparison of cell-tracking algorithms. Nat. Methods 14, 1141.

Weber, E., Engler, C., Gruetzner, R., Werner, S., Marillonnet, S., 2011. A modular cloning system for standardized assembly of multigene constructs. PLoS One 6, e16765.

Weber, K., Bartsch, U., Stocking, C., Fehse, B., 2008. A multicolor panel of novel lentiviral "gene

ontology"(LeGO) vectors for functional gene analysis. Mol. Ther. 16, 698–706.

Zong, H., Espinosa, J.S., Su, H.H., Muzumdar, M.D., Luo, L., 2005. Mosaic analysis with double markers in mice. Cell 121, 479–492.

Zou, K.H., Warfield, S.K., Bharatha, A., Tempany, C.M.C., Kaus, M.R., Haker, S.J., Wells, W.M., Jolesz, F.A., Kikinis, R., 2004. Statistical validation of image segmentation quality based on a spatial overlap index1: scientific reports. Acad. Radiol. 11, 178–189.

**Table 1.** Performance of the proposed method in the cell detection. TP: True Positive, FP: False Positive, FN: False Negative.

| Validation | TP | FP | FN | Recall | Precision | F1_SCORE |
|---|---|---|---|---|---|---|
| OP1 vs OP2 | 352 | 28 | 27 | 0.9288 | 0.9263 | 0.9275 |
| OP1 vs FAST | 337 | 29 | 43 | 0.8868 | 0.9207 | 0.9034 |
| OP2 vs FAST | 341 | 24 | 39 | 0.8974 | 0.9342 | 0.9154 |

**Table 2.** Accuracy of the proposed method in the segmentation and labeling of cells. Data are reported as mean ± standard deviation. (*) denotes statistically difference. SDC: Sorensen-Dice Coefficient, HD: Hausdorff Distance.

| Validation | SDC | HD ($\mu m$) | CCA (%) |
|---|---|---|---|
| OP1 vs OP2 | 0.9385± 0.0231 | 0.8088 ± 0.0898 | 96.25 ± 1.84 |
| OP1 vs FAST | 0.9339 ± 0.0430 | 0.9232 ± 0.0747 (*) | 96.42 ± 2.19 |
| OP2 vs FAST | 0.9335 ± 0.0467 | 1.0403 ± 0.5650 (*) | 96.35 ± 2.14 |

**Table 3.** Color Agreement between the two operators (OP1, OP2) and the proposed bethod for each of the six fluorescent channels.

| Color Agreement | RED | ORANGE | YELLOW | GREEN | CYAN | BLUE |
|---|---|---|---|---|---|---|
| OP1 vs FAST | 97.71 % | 94.97 % | 97.26 % | 97.26 % | 91.78 % | 100 % |
| OP2 vs FAST | 96.09 % | 94.79 % | 96.69 % | 98.59 % | 92.09 % | 99.09 % |

**Table 4.** Performance of two open-source software (CellProfiler, Fiji) in the cell detection. TP: True Positive, FP: False Positive, FN: False Negative.

| Method | Computational time (sec) | TP | FP | FN | Recall | Precision | F1_SCORE |
|---|---|---|---|---|---|---|---|
| OP1 vs CellProfiler | 18.54 ± 4.84 | 234 | 4 | 146 | 0.6157 | 0.9831 | 0.7571 |
| OP2 vs CellProfiler | | 227 | 5 | 153 | 0.5974 | 0.9784 | 0.7418 |
| OP1 vs Fiji | 38.78 ± 5.47 | 339 | 15 | 41 | 0.8921 | 0.9576 | 0.9236 |
| OP2 vs Fiji | | 336 | 19 | 44 | 0.8842 | 0.9465 | 0.9143 |
| **OP1 vs FAST** | **5.11 ± 1.21** | **337** | **29** | **43** | **0.8868** | **0.9207** | **0.9034** |
| **OP2 vs FAST** | | **341** | **24** | **39** | **0.8974** | **0.9342** | **0.9154** |

**Table 5.** Accuracy of two open-source software in the segmentation of neuronal cellular clones. Data are reported as mean ± standard deviation. SDC: Sorensen-Dice Coefficient, HD: Hausdorff Distance.

| *Method* | *SDC* | *HD ($\mu m$)* |
|---|---|---|
| *OP1 vs CellProfiler* | 0.8371 ± 0.0781 | 1.8347 ± 1.5377 |
| *OP2 vs CellProfiler* | 0.8234 ± 0.0866 | 1.8796 ± 1.5186 |
| *OP1 vs Fiji* | 0.9021 ± 0.0814 | 1.6811 ± 1.3259 |
| *OP2 vs Fiji* | 0.8946 ± 0.0859 | 1.6735 ± 1.6564 |
| **OP1 vs FAST** | 0.9339 ± 0.0430 | 0.9232 ± 0.0747 |
| **OP2 vs FAST** | 0.9335 ± 0.0467 | 1.0403 ± 0.5650 |

**Table 6.** Sensitivity analysis of the three main FAST parameters: $polynomial_{ORDER}$, $small_{OBJECTS}$ and $num_{CONDITIONS}$. Performance was evaluated by comparing manual annotation with the automatic segmentation (OP1 vs. FAST, OP2 vs. FAST). The optimal value for each parameter is highlighted in boldface.

| *Parameter* | *Value* | *OP1 vs FAST ($F1_{SCORE}$)* | *OP2 vs FAST ($F1_{SCORE}$)* |
|---|---|---|---|
| $polynomial_{ORDER}$ | 3 | 0.8521 | 0.8483 |
| | **5** | **0.9034** | **0.9154** |
| | 7 | 0.8167 | 0.8380 |
| $small_{OBJECTS}$ | 2.86 μm$^2$ (20 pixel$^2$) | 0.7349 | 0.7451 |
| | **7.15 μm$^2$ (50 pixel$^2$)** | **0.9034** | **0.9154** |
| | 14.30 μm$^2$ (100 pixel$^2$) | 0.8624 | 0.8557 |
| $num_{CONDITIONS}$ | 4/6 | 0.7895 | 0.7953 |
| | **5/6** | **0.9034** | **0.9154** |
| | 6/6 | 0.8629 | 0.8584 |

28